Response of Inconel 617 to Sea Salt and Re-entry Conditions

Ronald K. Clark*
NASA Langley Research Center, Hampton, Virginia
and
Jalaiah Unnam†
Analytical Services and Materials Inc., Hampton, Virginia

Inconel 617 is a nickel-based superalloy being considered for heat-shield applications because of its high-temperature strength, good oxidation resistance, and high emittance of oxidized surfaces. While the effects of simulated re-entry conditions on emittance and oxidation of Inconel 617 have been studied, the combined effects of the ground-based environment with sea salt exposure and the re-entry environment have not been evaluated. Experimental results are presented to show the effects of environmental simulation including ground-based and re-entry exposure on the emittance and oxidation of Inconel 617. Specimens were exposed to simulated re-entry at a surface temperature of 1370 K in the Langley Research Center Hypersonic Materials Environmental Test System Facility with and without alternate exposures to an atmospheric seashore environment or a laboratory sea salt environment. This paper presents emittance, mass loss, oxide chemistry, and alloy composition data for the specimens.

Introduction

THE metallic heat-shield concept continues to be of strong interest for the radiatively cooled thermal protection system (TPS) for advanced reusable space transportation vehicles[1] and hypersonic aircraft.[2] Nickel-chromium superalloys in general have been shown to possess the desirable characteristics of high-temperature strength and excellent long-term oxidation resistance, which are prerequisites to successful performance of metallic TPS.[3-8] In addition, efficient radiative TPS must have a high, stable emittance for up to 100 flights. Inconel 617 has been shown to meet the high-temperature strength/oxidation resistance criteria and its surface has a relatively high emittance (about 0.8) for up to 100 exposure cycles.[9-11] However, the response of Inconel 617 to the more realistic environment that couples ground-based exposure, including the presence of sea salt, with space transportation system (STS) re-entry exposure has not been examined.

Concerns for the effects of sea salt exposure on the performance of Inconel 617 in TPS applications are heightened by results from hot corrosion studies of superalloys in engine applications.[12,13] Burner rig tests of Inconel 617 in the presence of sea salt contamination showed hot corrosion with severe intergranular attack at 1170 K.[12] The hot corrosion results from Na_2SO_4, which is present to some degree in sea salt and is a product of the reaction of NaCl (the principal constituent of sea salt), and the oxides of sulfur that are present in most fuels.[13] The service environment of advanced STS vehicles would necessarily include exposure of surfaces to sea salt with a buildup of crystals. Those salt deposits combined with the high surface temperature encountered during re-entry to the Earth's atmosphere have the potential to produce harmful effects to the vehicle surface.

The purpose of this research was to define the effects of combined ground-based and STS re-entry exposure on the emittance and oxidation characteristics of Inconel 617. The oxidation characteristics of interest relate to the type and quantity of oxides formed at the exposed surface and their effect on surface-radiating properties of the alloy. Variations in the alloy microstructure with exposure conditions were not examined. Specimens were exposed to simulated re-entry at a surface temperature of 1370 K in the Langley Research Center, Hypersonic Materials Environmental Test System (HYMETS) Facility with and without alternate exposures to a seashore environment or a laboratory sea salt environment.

Experimental Procedures

Test Specimens

Test specimens were stamped from an 0.8-mm-thick sheet of Inconel 617. The specimens were disks 2.5 cm in diameter with three 0.5×0.5 cm radial projections spaced every 120 deg around the disk for mounting the specimens during re-entry exposure. Table 1 gives the chemical analysis of the material as provided by the certification-of-test report from the vendor.

Exposure of Specimens

Specimens were statically oxidized for 12 h at 1260 K in laboratory air to give a high emittance before the start of re-entry testing. Prior to static oxidation, the specimens were thoroughly cleaned to assure that they were free of oils.

Specimens were exposed to cyclic conditions of simulated STS re-entry with and without alternate exposures to a seashore environment or a laboratory sea salt environment. The simulated re-entry tests were half-hour exposures at a surface temperature of 1370 K in the Langley Research Center HYMETS Facility. The seashore environmental tests were two-week exposures on a specimen rack located at the east end of the Langley Air Force Base runway about 30 m from a salt-water inlet from the Chesapeake Bay in Hampton, Virginia. The laboratory sea salt tests were 24- to 72-h exposures where the specimens were dipped in sea water and then hung over the sea water bath in a closed container. The sea water used in the laboratory tests was taken from the inlet near the ground exposure site. Table 2 gives a chemical analysis of the sea water.

The HYMETS Facility is a 100-kW constrictor arc-heated wind tunnel.[14] Figure 1 shows a schematic diagram of the test setup. It consists of a segmented constrictor-arc heater, a test chamber with three model insertion stings, and continuous duty vacuum pumps. Specimens are mounted on stagnation model adaptors attached to the insertion strings. Another

Presented as Paper 84-1768 at the AIAA 19th Thermophysics Conference, Snowmass, CO, June 25-28, 1984; submitted Aug. 15, 1984; revision received July 8, 1985. This paper is declared a work of the U.S. Government and therefore is in the public domain.

*Research Scientist. Member AIAA.
†Senior Scientist.

Table 1 Inconel 617 analysis

Element	wt. %
Ni	53.20
Cr	22.63
Co	12.33
Mo	9.38
Al	1.15
Fe	0.76
Ti	0.27
Si	0.15
C	0.06
Cu	0.05
Mn	0.02
S	0.001

Table 2 Sea water analysis

Component	
Boron,[a] g/liter	< 0.005
Sodium, g/liter	11.0
Chloride, g/liter	9.8
Magnesium, g/liter	1.8
Sulfate, g/liter	1.5
Calcium, g/liter	0.01
Potassium, g/liter	0.22
Fluoride, g/liter	0.0006
Bromide, g/liter	< 0.1
Barium, mg/liter	< 0.05
Manganese, g/liter	< 0.01
Copper, mg/liter	0.010
Zinc, mg/liter	0.025
Lead, mg/liter	< 0.002
Silver,[b] mg/liter	< 0.002
Nitrate, mg/liter	0.02
Chlorinity	3.90
pH	7.6
Carbonate (as $HCO3^-$), g/liter	0.037

[a]Boron detection limit was 0.005 g/liter. [b]Silver detection limit was 0.002 mg/liter.

Table 3 HYMETS operating conditions for simulated STS re-entry exposure of specimens

Specimen surface temperature, K	1370
Surface pressure, Pa	630
Freestream Mach No.	3.3
Freestream enthalpy, MJ/kg	5.6
Cold wall heating rate, kW/m^2	200-230

sting contains a water-cooled heating rate/pressure probe used to measure the cold wall heating rate and the surface pressure. The test gas is a mixture of air plus nitrogen and oxygen in ratios equivalent to air. High-purity nitrogen is introduced at the downstream end of the cathode. Air and high-purity oxygen are introduced in the plenum and mixing chamber.

The nominal operating conditions for simulated re-entry testing of the specimens are given in Table 3. The test conditions utilized here do not provide for full simulation of the advanced STS re-entry environment. The heat flux—the most critical response parameter—is representative of the re-entry environment, but the surface pressure and freestream enthalpy are one-half to one-fourth the levels encountered on re-entry.

Analyses of Oxidation

Mass changes of specimens were determined by weighing specimens after the initial static oxidation and after each re-entry cycle. The mass change data were used to estimate substrate thickness changes and as a basis of comparison for specimens with different exposure conditions.

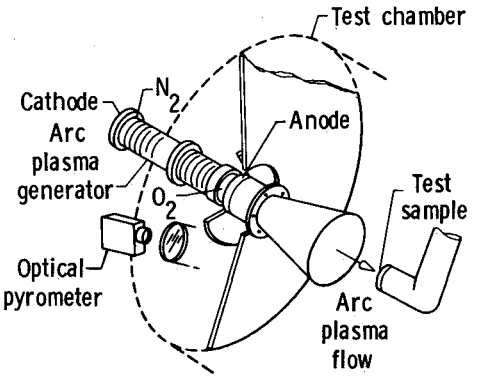

Fig. 1 Langley Research Center HYMETS Facility for simulated re-entry testing.

The morphology of specimen oxides was studied using conventional light microscopy and scanning electron microscopy (SEM) at magnifications up to 1500×. The oxide composition was analyzed by energy dispersive x-ray analysis (EDAX), x-ray diffraction analysis (XRD), and electron microprobe analysis (EMP).

Microprobe analyses of polished cross sections of oxidized specimens were performed to determine the substrate elemental composition profiles. Composition analyses were conducted at known locations beginning at the oxide-substrate interface and progressing to the interior. The microprobe was also used to determine the oxide thickness by making line scans across the polished cross sections.

Radiative Property Measurement

Room temperature near-normal reflectance measurements were made on pre- and post exposure specimens using a Gier-Dunkle DB100 reflectometer and a Gier-Dunkle Model HCDR-3 heated-cavity reflectometer (HCDR). The DB100 reflectometer measures the total room temperature reflectance. The heated-cavity reflectometer was used to make spectral reflectance measurements over the wavelength range of 2-25 μm. The reflectance data were used with Kirchoff's law to arrive at corresponding values of emittance. The spectral data were integrated with respect to the Planck blackbody energy distribution curve for 1370 K to arrive at the total normal emittance at 1370 K.

A limited number of near-normal spectral emittance measurements were made at 1370 K for comparison with the emittance data derived from reflectance measurements. The spectral emittance measurements were made over the wavelength range of 1-15 μm using a radiometric technique.[15]

Results and Discussion

Table 4 presents a summary of the mass loss and emittance results for combined ground-based and re-entry exposure of Inconel 617. Data are shown for specimens in the statically oxidized condition after exposure to 1) simulated re-entry, 2) combinations of re-entry and atmospheric or laboratory sea salt conditions, and 3) simulated re-entry with oxide removal.

Oxidation Characteristics

The oxidation characteristics of nickel-chromium alloys under the dynamic oxidation conditions of STS re-entry are significantly different from the oxidation characteristics under static oxidation conditions. The presence of atomic oxygen and the high-speed flow conditions of re-entry result in accelerated rates of removal of oxides at the surface. Chromium, which is present as Cr_2O_3 in the surface oxide, is particularly susceptible to removal by vaporization and oxidation. Removal of these oxides represents a loss in mass by the alloy.

The mass loss data in Table 4 for tests up to 10 cycles are shown graphically in Fig. 2. Each data point represents a loss

Table 4 Summary of results for combined ground-based and re-entry exposure of Inconel 617

Specimen No.	Exposure condition[a]	No. of cycles	Heating rate, kW/m^2	Surface pressure, Pa	Stream enthalpy, MJ/kg	Mass loss, mg/cm^2	Total emittance: Room temperature HCDR	Room temperature DB100	1370 K HCDR	1370 K HTEA
I-227	AR	–	–	–	–	–	0.68	0.68	0.86	0.82
I-208	R	1	211	627	5.6	1.24	0.77	0.76	0.90	–
I-209	R	1	193	640	5.1	1.40	0.78	0.77	0.90	–
I-219	R	3	203	640	5.4	2.04	0.81	0.80	0.89	–
I-221	R	3	216	–	5.7	1.96	0.82	0.80	0.89	–
I-229	R	6	–	640	–	2.62	0.84	–	0.87	–
I-231	R	6	–	–	–	2.88	0.86	0.83	0.87	–
I-11	R	10	–	–	–	–	0.85	0.83	0.87	–
I-15	R	10	–	–	–	–	0.90	0.88	0.79	–
I-211	R	10	–	–	–	3.45	0.87	0.85	0.89	–
I-220	R	10	–	–	–	3.40	0.86	–	0.80	–
I-223	R	10	202	627	5.4	2.89	0.86	0.83	0.87	0.83
I-224	R	10	208	627	5.5	2.91	0.84	–	0.88	–
I-19	R	31	–	–	–	–	0.91	0.89	0.80	–
I-20	R	31	–	–	–	–	0.92	0.89	0.80	–
I-222	R	52	243	627	6.9	11.98	0.91	–	0.74	–
I-448	R	50	271	653	7.6	13.79	0.93	–	0.76	–
I-478	R	50	267	640	7.5	13.87	0.93	–	0.76	–
I-202	RL	2	193	640	5.1	1.57	0.81	0.79	0.88	–
I-205	RL	3	204	613	5.5	2.03	0.84	0.82	0.87	–
I-216	RL	6	–	–	–	3.08	0.81	–	0.81	–
I-213	RL	10	–	–	–	4.39	0.80	–	0.81	–
I-454	RL	50	271	640	7.6	26.19	0.85	–	0.65	–
I-476	RL	50	271	653	7.6	28.23	0.84	–	0.64	–
I-206	RA	2	225	640	5.9	1.72	0.80	0.79	0.89	–
I-204	RA	5	194	600	5.3	2.78	0.82	–	0.88	–
I-214	RA	5	227	640	6.0	3.04	0.84	–	0.86	–
I-210	RO	5	191	587	5.3	3.07	0.84	0.82	0.88	–
I-212	RO	10	236	587	6.7	4.91	0.86	–	0.87	–
I-203	ROX	10	196	613	5.3	–	0.73	0.73	0.82	–

[a]Exposure conditions: AR = statically oxidized for 12 h at 1260 K, furnace cooled; R = simulated re-entry at 1370 K surface temperature; RL = simulated re-entry with laboratory exposure to seasalt; RA = simulated re-entry with atmospheric exposure to sea salt; RO = simulated re-entry with mechanical removal of oxide between cycles; ROX = simulated re-entry with mechanical removal of oxide after 10 cycles.

in mass with exposure compared to short-time static oxidation data for Inconel 617, which shows a mass increase of about 0.1 mg/cm^2 after 5 h of static oxidation at 1370 K.[16] The data for the exposure condition designated "re-entry with oxide removal" represents the "worst case" for mass loss since the oxide was removed with a stiff bristle brush after each simulated re-entry cycle. The "mildest case" is the exposure consisting of simulated re-entry with no sea salt exposure. The difference in mass loss for these extremes increases with the number of exposure cycles. Beyond four exposure cycles, specimens subjected to atmospheric and laboratory sea salt conditions experience a slightly greater mass loss than specimens subjected to simulated re-entry with no sea salt exposure.

Extended-duration re-entry simulation tests of specimens with and without laboratory sea salt exposure were conducted for up to 52 simulation exposure cycles (Table 4). Specimens from each test condition continued to experience a loss in mass throughout the sequence of exposure cycles. The rate of mass loss for specimens from both test conditions was about linear with time after an initial stabilizing period of about five cycles. After 50 cycles of exposure, the total mass loss of specimens subjected to laboratory-simulated re-entry with sea salt exposure is about double the mass loss of specimens subjected to re-entry without sea salt exposure.

Figure 3 shows SEM photographs of the surface oxides of specimens for different exposure conditions. The statically formed oxide (Fig. 3a) is flat and uniform, much like the faceted structure of unoxidized Inconel 617. SEM photographs of specimens after simulated re-entry with and without sea salt exposure (Figs. 3b and 3c) show spherical oxide particles at the surface, which are typical of the oxide morphologies reported in the literature for dynamically oxidized superalloys.[5,7,8,17] Evidence of disruption of the oxide by sea salt exposure is present in Fig. 3c, which shows some irregularities in the spherical oxide particles, and in Fig. 3d, which shows no spherical particles. The morphologies of specimens after extended-duration re-entry simulation tests are very similar to the morphologies of specimens after 10 exposure cycles.

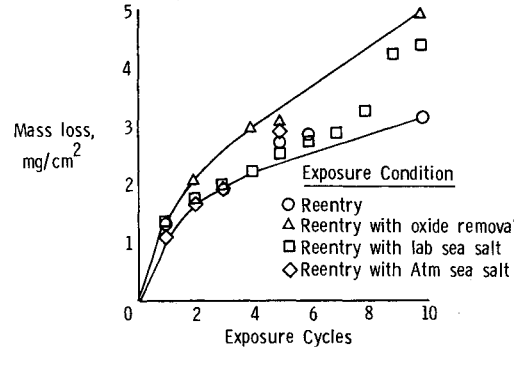

Fig. 2 Mass loss of Inconel 617 with TPS exposure.

The fragile nature of oxides of Ni-Cr alloy oxidized under dynamic conditions has been a cause for concern. The SEM photograph of the specimen after re-entry with atmospheric exposure shows that the oxide is weathered to the extent that the spherical oxide particles have been removed; however, the mass loss data in Fig. 2 show that the sea salt exposure specimens experienced only slightly greater mass loss than specimens exposed to re-entry alone.

Table 5 Summary of results from EDAX, XRD, and EMP analyses of specimens

		Surface analysis											EMP line scans	
		EDAX counts			XRD phases			EMP, wt. %						
Specimen No.	Exposure/ No. of cycles	Cr	Co	Ni	Cr_2O_3	$CoCr_2O_4$	NiO	Cr	Ni	Co	O	OET[a]	Oxide thickness, μm	Alloy depletion, μm
I-227	AR	–	–	–	Very strong			56	6	2	32	4	5	19
I-230	AR	80	1	4										
I-229	R/6												5	27
I-210	R/10	22	9	38									7	37
I-221	R/10				Strong	Weak	Strong							
I-223	R/10				Strong	Weak	Strong							
I-224	R/10	35 10[b] 58[c]	7 6[b] 4[c]	38 49[b] 11[c]				25	32	7	32	4		
I-448	R/50				Weak	Moderate	Very strong							
I-478	R/50												5	103
I-216	RL/6												5	31
I-213	RL/10	30	13	28	Strong	Weak	Strong	24	27	11	34	4	6	34
I-476	RL/50												3	119
I-204	RA/5												6	30
I-214	RA/5	27 5[b]	6 8[b]	19 41[b]	Strong	Very weak	Moderate							
I-212	RO/10	22	10	35	Strong	Weak	Strong						7	47

[a]Other elements total. [b]Spot analysis of spherical oxide particle. [c]Spot analysis of suboxide.

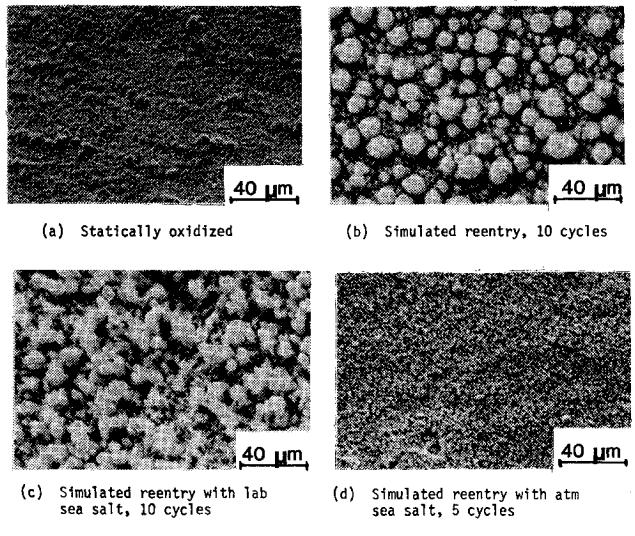

(a) Statically oxidized (b) Simulated reentry, 10 cycles

(c) Simulated reentry with lab sea salt, 10 cycles (d) Simulated reentry with atm sea salt, 5 cycles

Fig. 3 SEM photographs of Inconel 617 oxide surfaces.

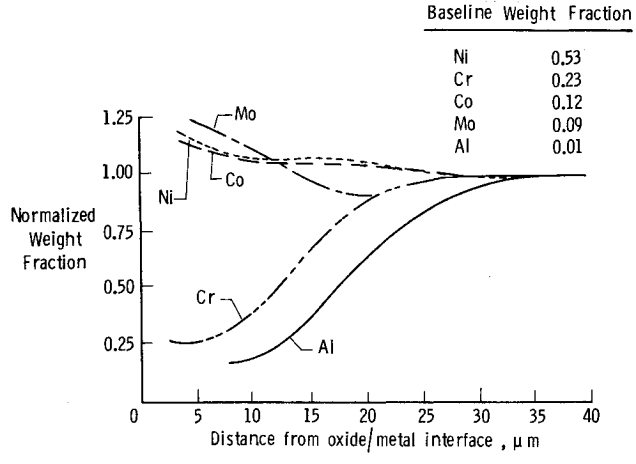

Fig. 4 Elemental composition profiles of Inconel 617 metal substrate.

Table 5 presents data from analysis of specimens using EDAX, XRD, and EMP. These data indicate that the statically formed oxide of Inconel 617 is Cr_2O_3. Specimens exposed to simulated re-entry have a high NiO content and a minor $CoCr_2O_4$ content in the surface oxide. The NiO exists primarily as spherical oxide particles on top of a Cr_2O_3-rich suboxide and the $CoCr_2O_4$ exists as a minor constituent in the suboxide.

The oxide chemistry data for specimens after sea salt exposure are not notably different from the data for specimens with no sea salt exposure. The absence of any evidence of chemical species characteristic of sea salt indicates that salt deposits from sea salt exposure are quickly volatilized on exposure to re-entry conditions and do not react with the surface oxide.

The microprobe line scan data in Table 5 show the oxide thickness and alloy depletion depth for a number of specimens. The oxide thickness ranges from 5 μm for the statically formed oxide to 6-7 μm for specimens after exposure to 10 re-entry cycles. Longer-duration tests result in reduced oxide thickness for specimens with and without sea salt exposure. The thicknesses of the oxide on the 50-cycle specimens with and without sea salt exposure are about 3 and 5 μm, respectively.

Chromium and aluminum are selectively oxidized on exposure to re-entry conditions resulting in an alloy-depletion zone near the surface where the composition varies from the base alloy chemistry. Figure 4 shows quantitative compositional analysis data for the metal substrate of a typical 10-cycle specimen. The zone affected by diffusion of metal atoms to the surface is about 35 μm thick. Cr has been reduced to one-fourth the base alloy level at the oxide-substrate interface. Aluminum is similarly reduced. Ni, Co, and Mo experience an increase in weight fraction at the interface due to the loss of Cr. EDAX indicates that Al migrates toward the surface region where it collects in the grain boundaries.

Diffusion of Cr continues throughout re-entry exposure such that the alloy-depleted zone grows with time. The data in Table 5 show that the depleted zone for short-duration tests (up to 10 cycles) ranges from 19 μm in depth for the statically oxidized specimen to 47 μm in depth for the most severe case of re-entry with oxide removal after each cycle. The alloy-depleted zone of specimens exposed to 10 cycles of re-entry with and without sea salt exposure was 30-35 μm in depth. The depth of the alloy-depleted zone of specimens exposed to 50

cycles of re-entry is >100 μm. Alloy-depletion zone thicknesses of the order seen here comprise about 15% of the total thickness of the specimens in this program, hence there remains a major portion of undisturbed alloy and there should be ample mechanical performance to meet the needs in TPS applications. In applications using very thin sheets (150-250 μm), the effect of alloy depletion on mechanical properties should be investigated.

Radiative Properties

Room temperature reflectance data obtained with the HCDR heated-cavity reflectance apparatus and the DB100 reflectometer were used to calculate independent values of emittance. Room temperature emittance data determined by the two techniques, which are reported in Table 4, are in good agreement.

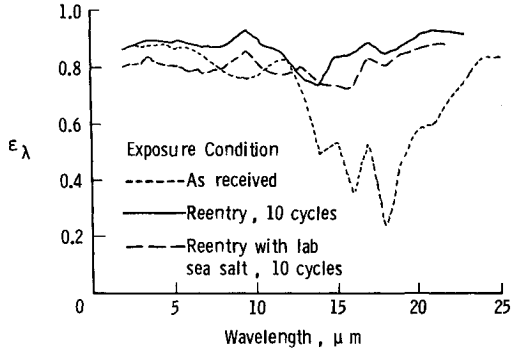

Fig. 5 Spectral emittance of Inconel 617 at room temperature.

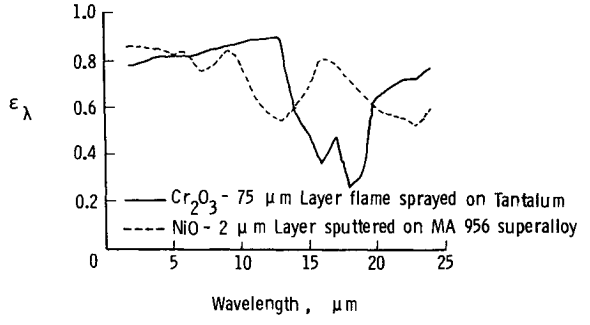

Fig. 6 Spectral emittance of oxides of Inconel 617 at room temperature.

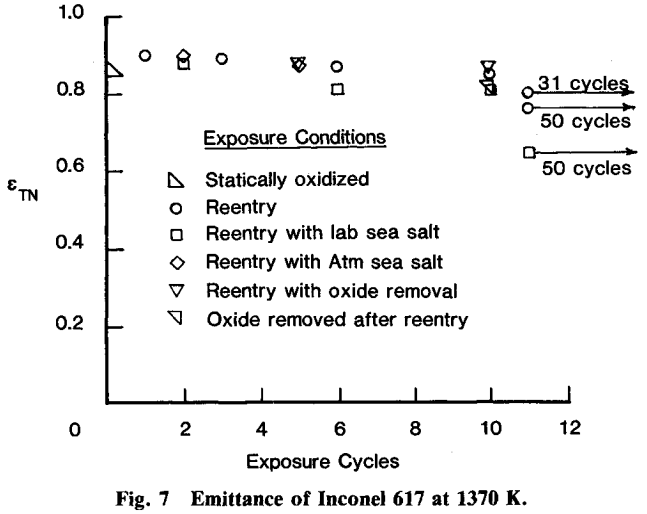

Fig. 7 Emittance of Inconel 617 at 1370 K.

Table 4 also reports 1370 K emittance values calculated from the HCDR spectral data, and two values of emittance measured at 1370 K using the NASA Langley Research Center high-temperature emittance apparatus (HTEA). The HTEA results are 0.04 less than the calculated values. Reference 11 reported the 1370-K emittance of statically oxidized Inconel 617 to be 0.84. Comparable data obtained in this program using the HCDR and HTEA are 0.86 and 0.82, respectively. These favorable comparisons support the use of room temperature spectral reflectance data to estimate the elevated temperature emittance of Inconel 617.

The effect of exposure conditions on normal spectral emittance of Inconel 617 is shown in Fig. 5. Spectral emittance data for statically oxidized specimens and for specimens after both 10-cycle re-entry exposure conditions are about 0.8 and higher over the wavelength range of 2-12 μm. The spectral emittance data for specimens after both 50-cycle exposure conditions are significantly lower than 0.8 in the shorter wavelength region. The spectral emittance data for the statically oxidized specimen has a strong dip in the wavelength range from 12 to 25 μm. The differences in emittance of the statically oxidized specimen and the specimens exposed to re-entry conditions are thought to result from the changes that occur in the surface oxide with re-entry exposure.

Figure 6 shows the spectral emittance of Cr_2O_3 and NiO—the primary oxides of Inconel 617. The emittance of Cr_2O_3 is very similar to the emittance of the statically oxidized specimen (Fig. 5). The spectral emittance of NiO has a peak in the wavelength range from 12 to 20 μm. As the fraction of NiO in the surface oxide increases with exposure to re-entry conditions, the emittance of the surface assumes more of the characteristics of NiO and Cr_2O_3 shown by the data in Fig. 5.

Since the radiative heat shield functions at elevated temperature, its radiative properties at temperatures of the order experienced during re-entry are of primary interest. Figure 7 shows the calculated total normal emittance for 1370 K vs exposure cycles for different conditions. The emittance is greater than 0.8 for all exposure conditions up to 10 cycles. The emittance of extended-duration exposure specimens is significantly lower than for the short-time exposure specimens. After 50 simulated re-entry cycles with laboratory sea salt exposure, the emittance is 0.64 compared to an emittance value of 0.75 for specimens with no sea salt exposure.

Concluding Remarks

The response of Inconel 617 to simulated re-entry with and without exposures to a seashore environment or a laboratory sea salt environment was studied and the following results were obtained.

1) There was no observable interaction between sea salt and the surface oxides of Inconel 617. The response of specimens subjected to re-entry simulation testing with sea salt exposure was not significantly different from specimens exposed to re-entry simulation alone. Any sea salt deposits at the oxide surface are volatilized very quickly during re-entry testing leaving no residue.

2) The elevated temperature emittance of Inconel 617 was greater than 0.8 for all exposure conditions and times up to 10 cycles. Tests for 50 cycles resulted in emittance values as low as 0.64.

3) Inconel 617 specimens exposed to simulated re-entry experience a loss of mass due to vaporization and oxidation of material at the surface. Cr, which is present in the surface oxide, is particularly susceptible to removal. The total loss of mass by specimens subjected to simulated re-entry with sea salt exposure is about double the mass loss by specimens subjected to simulated re-entry without sea salt exposure.

4) The oxide layer of statically oxidized Inconel 617 is about 5 μm thick and consists primarily of Cr_2O_3. The oxide thickness of Inconel 617 exposed to simulated re-entry with or without sea salt is about 6 μm and consists of NiO and Cr_2O_3 with minor traces of $CoCr_2O_4$. The oxide thicknesses of

50-cycle specimens with and without sea salt exposure are 3 and 5 μm, respectively.

5) Selected diffusion of metal atoms from the alloy substrate to the oxide metal interface results in an alloy-depleted zone that ranges from 19 μm in thickness for a statically oxidized specimen to 45 μm for a specimen exposed to 10 cycles of simulated re-entry with the oxide removed between re-entry cycles. The thickness of the alloy-depleted zone of specimens exposed to 10 cycles of simulated re-entry with or without sea salt exposure is 30-35 μm. The thickness of the alloy-depleted zone of 50-cycle specimens is greater than 100 μm.

References

[1]Jackson, L.R. and Dixon, S.C., "A Design Assessment of Multiwall, Metallic Stand-Off, and RSI Reusable Thermal Protection Systems Including Space Shuttle Applications," NASA TM-8170, April 1980.

[2]Taylor, A.H. and Jackson, L.R., "Thermostructural Analyses of Structural Concepts for Hypersonic Cruise Vehicles," AIAA Paper 80-0407, Jan. 1980.

[3]Devikis, W.D., Miserentino, R., Weinstein, I., and Shideler, J.L., "Aerothermal Performance and Structural Integrity of a Rene' 41 Thermal Protection System in a Mach 6.6 Stream," NASA TN D-7943, 1975.

[4]Gilbreath, W.P., "Degradation of Space Shuttle TPS Metals in Dissociated Oxygen," AIAA Paper 72-262, April 1972.

[5]Tenney, D.R., Young, C.T., and Herring, H.W., "Oxidation Behavior of TD-NiCr in a Dynamic High Temperature Environment," *Metallurgical Transactions,* Vol. 5, May 1974, pp. 1001-1012.

[6]Schaffer, J.W. et al., "Analytical and Experimental Evaluation of Flowing Air Test Conditions for Selected Metallics in a Shuttle TPS Application," NASA CR-2531, Aug. 1975.

[7]Young, C.T., Tenney, D.R., and Herring, H.W., "Dynamic Oxidation Behavior of TD-NiCr Alloy with Different Surface Pretreatments," *Metallurgical Transactions,* Ser. A., Vol. 6A, Dec. 1975, pp. 2253-2265.

[8]Clark, R.K., Webb, G.L., and Dries, G.A., "Mechanical/Radiative Performance of Rene' 41 in TPS Applications," *Advances in TPS and Structures for Space Transportation Systems,* compiled by H. Neale Kelly and James E. Gardner, NASA CP-2315, 1984, pp. 361-380.

[9]Norris, B., "High Temperature [1366K (2000°F)] Sheet Material Selection for Use for Thermal Protection Systems," Rept. RHR 80-917, ROHR Industries, Chula Vista, CA, April 1980.

[10]Cunnington, G.R., Fretter, E.F., and Clark, R.K., "Radiative Properties of a Nickel Based Superalloy—Inconel 617—After Simulated Earth Reentry," AIAA Paper 82-0898, June 1982.

[11]Cunnington, G.R., Funai, A.I., and McNab, T.K., "Radiative Properties of Advanced Spacecraft Heat Shield Materials," NASA CR-3740, Nov. 1983.

[12]Santoro, G.J., "Hot Corrosion of Four Superalloys: HA-188, S-57, In-617, and TD-NiCrAl," *Oxidation of Metals,* Vol. 13, No. 5, 1979, pp. 405-435.

[13]Bornstein, N.S., DeCrescente, M.A., and Roth, H.A., "Effect of Vanadium and Sodium Compounds on the Accelerated Oxidation of Nickel Base Alloys," *Proceedings of the 1974 Gas Turbine Materials in the Marine Environment Conference,* July 1974, MCIC-75-27, 1974, pp. 115-160.

[14]Foster, T., "Modification to the NASA LaRC/Aerotherm 100-kW Arc-Heated Wind Tunnel System," NASA CR-77262, Sept. 1977.

[15]Edwards, S.F., Kantsios, A.G., Voros, J.P., and Stewart, W.F., "Apparatus Description and Data Analysis of a Radiometric Technique for Measurement of Spectral and Total Normal Emittance," NASA TN D-7798, 1975.

[16]Hosier, J.C. and Tillack, D.J., "Inconel Alloy 617—A New High Temperature Alloy," *Metals Engineering Quarterly,* Aug. 1972.

[17]Clark, R.K., Dicus, D.L., and Lisagor, W.B., "Emittance of TD-NiCr After Simulated Reentry Heating," *Thermal Conductivity 15,* edited by Vladimir V. Mirkovich, Plenum Press, New York, 1978, pp. 343-353.